energies

MDPI

Communication

A Theoretical Model for Voltage-Dependent Photocurrent Collection in CdTe Solar Cells

Cindy X. Zhao * and Ken K. Chin

CNBM New Energy Materials Research Center, New Jersey Institute of Technology, Newark, NJ 07102, USA; chin@njit.edu

* Correspondence: zhaox8@mcmaster.ca

Abstract: The classic solar cell model assumes that the photo-generated current is a constant, independent of the cell's output voltage. Experimental data of CdTe solar cells, however, show that the photocurrent collection efficiency decreases with the increase of the cell's output voltage. In this work, we proposed a theoretical model for the CdTe thin-film cell, which assumes that the loss of photocurrent in the CdTe absorber is primarily due to the minority carrier recombination in the neutral region and at the back contact. By solving the neutral region's diffusion equation, with proper boundary conditions, we have obtained the analytical expressions of the photocurrent collection efficiency and the cell's J-V performance. Our theoretical results agree well with the experimental data. According to our theoretical model, the CdTe thin-film solar cell has an optimized p-doping level. A higher doping density may not be always good for a CdTe solar cell due to the reduced depletion width and decreased photocurrent at normal operation voltage, although the higher doping density can improve the open-circuit voltage by increasing built-in voltage.

Keywords: photocurrent; CdTe solar cells; collection loss

Citation: Zhao, C.X.; Chin, K.K. A Theoretical Model for Voltage-Dependent Photocurrent Collection in CdTe Solar Cells. *Energies* **2021**, *14*, 1615. https://doi.org/10.3390/en14061615

Academic Editor: Ricardo J. Bessa

Received: 4 February 2021
Accepted: 10 March 2021
Published: 15 March 2021

1. Introduction

In thin-film solar cells, photocurrent collection losses can be extremely significant due to their high absorption coefficient, short absorption lengths, small depletion widths, and short diffusion lengths [1]. Voltage-dependent photocurrent collection losses have been observed in all thin-film solar cells, including those based on Cu_2S, $CuInSe_2$, CdTe, organic P3HT/PCBM, and inorganic III-V solar cells [2–6]. The physical model of classic silicon solar cells assumes that the photo-generated current is a constant, independent of the cell's output voltage. Unlike their crystalline silicon counterpart, the principle of superposition and the shift of dark current downwards by a constant photocurrent do not work for these thin-film solar cells [7–9]. Therefore, the classical five-parameter model fails to describe the J-V characteristics of CdTe solar cells, especially in the range of forward bias close to V_{oc} [10]. The actual J-V curve of a CdTe thin-film solar cell shows: (1) in the low forward bias region, the current changes with photon flux, (2) the photo-carrier collection depending on the voltage applied, and (3) in some of the devices with large ohmic series resistance and poor performance, the S-kink behavior [11,12]. To unveil the reason, there is much literature that reports the bulk and interfacial recombination from both experiments and calculations [13–15], involving complicated and interdependent physical elements.

To obtain a more direct view and find a better theoretical model, in this work, we introduced a very simple analytical expression for photocurrent collection whereby recombination in the neutral region is taken into account. We assumed that the loss of photocurrent in the CdTe absorber is primarily due to the minority carrier recombination in the neutral region and at the back contact. The most important parameters in our model are the absorption length, depletion region width, and diffusion length. We solved the diffusion equation with boundary conditions in CdTe solar cells and obtained the analytical expressions of the bias-dependent photocurrent collection and the cell's J-V performance.

The diffusion length/doping density dependence of the photocurrent was validated against both simulation and experimental data in forward bias.

2. Modeling

2.1. CdTe Solar Cell Structure

In this work, the structure of a typical CdTe solar cell is based on the superstrate concept [16]. The incident sunlight hits the glass substrate, followed by the transparent front contact (i.e., TCO), n-type CdS (window layer), p-type CdTe (absorber), and metal back contact. Accordingly, we define and summarize parameters used in our model, as shown in Figure 1.

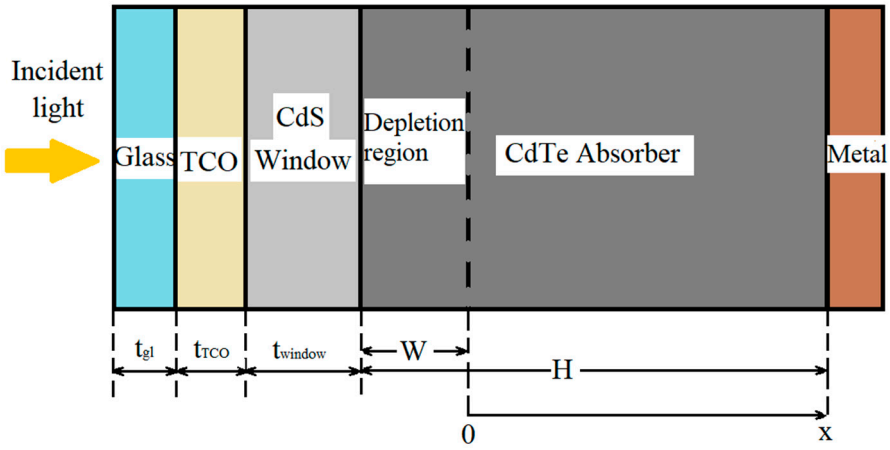

Figure 1. CdTe solar cell structure with a defined thickness for each layer, that is, t_{gl}, t_{TCO}, t_{window}, and H represent the thickness of glass, TCO layer, CdS window layer, and CdTe absorber layer, respectively. x is defined as any position in the neutral region, thus $x = 0$ is set to be at the depletion region edge, and $x = H - W$ at the metal back contact.

2.2. Optical Condition in CdTe Solar Cells

The spectrum of the sunlight incident on the terrestrial solar cell or module is expressed by standard $I_{AM1.5}(E)$, which has the dimension of W/m^2 eV. Air Mass 1.5 (AM 1.5) indicates $\cos\theta = \frac{1}{1.5}$, θ being the incident angle of the sunlight with respect to the normal of the Earth's surface. Therefore, the photon flux density of the incident light with photon energy greater than the absorber's bandgap is expressed as

$$\phi_{AM1.5} = \int_{h\upsilon \geq E_G}^{\infty} \frac{I_{AM1.5}(E)dE}{E} \tag{1}$$

The photon flux $\phi_{AM1.5}$ is partially reflected, and absorbed by the glass, TCO, and window layers, and the photon flux density, with $E \geq E_G$, incident on the CdTe absorber surface is

$$\phi_0 = \phi_{AM1.5}(1 - R)\exp\left(-\frac{t_{gl}}{L_{gl}}\right)\exp\left(-\frac{t_{TCO}}{L_{TCO}}\right)\exp\left(-\frac{t_{window}}{L_{window}}\right) \tag{2}$$

where the superstrate glass reflectance R and optical absorption length of the glass, TCO, and window layers L_{gl}, L_{TCO}, and L_{window} are averaged through the photon energy spectrum.

2.3. Electrical Conditions in CdTe Solar Cells

Our model, developed for CdTe solar cells, represents a solution to the continuity equation assuming complete photocurrent collection in the depletion region. Thus, the

main recombination is considered to occur in the neutral region of the absorber and possibly at interfaces, which will be further discussed in Section 3.

Based on the low injection assumption, the photo-generated electron density n in the neutral region of CdTe obeys the diffusion equation:

$$D_n \frac{d^2\Delta n}{dx^2} - \frac{\Delta n}{\tau_n} = -\frac{1}{L_a}\phi_0 \exp\left(-\frac{W}{L_a}\right) \exp\left(-\frac{x}{L_a}\right) \quad (3)$$

where the optical absorption length L_a is the weighted average of the photon energy dependent absorption length, D_n the diffusivity, and τ_n the lifetime of charge carrier. The dependence of depletion width W on the output voltage V is described as

$$W = \sqrt{\frac{2\varepsilon\varepsilon_r(V_{bi} - V)}{qN_A^-}} \quad (4)$$

With ε and ε_r being the dielectric constant, V_{bi} the built-in voltage of the CdS-CdTe heterojunction, and the number of ionized dopants $N_A{}^-$ [17]. Considering the fact that the activation energies of the dopant levels are non-shallow in CdTe [18], the dopants are partially ionized and the number of ionized dopants $N_A{}^-$ can be expressed by [19]:

$$p = N_V \exp(\frac{E_V - E_F}{kT}) = N_A^- = N_A \frac{1}{1 + 4\exp(\frac{E_A - E_F}{kT})} \quad (5)$$

where E_A is the transition energy level.

$$V_{bi} = E_g - \Delta E_c - \Delta E_n - \Delta E_p \quad (6)$$

where E_g is the bandgap of CdTe with a value of 1.5 eV [17,20], the offsets of energy level ΔE_c and ΔE_n of 0.1 eV in CdS-CdTe heterojunction, and ΔE_p the offset of Fermi level in p-CdTe. Assuming there is a single dopant in p-type CdTe, Cu substitute of Cd $Cu_{Cd}{}^{(0/-)}$ with the transition energy level of 0.22 eV, and density of states in p-type CdTe N_v =1.8 × 10^{19} cm^{-3}, the calculated Fermi level E_F, $N_A{}^-$, and V_{bi} are listed in Table 1 for CdTe solar cells with different CdTe doping densities N_A ranged from 10^{14} to 10^{17} cm^{-3}. Due to the non-shallow activation energy levels of the Cu dopants in CdTe, the hole density is a few orders lower than the acceptor concentration. The finding is further supported by the calculation of p-doping limit and donor compensation in CdTe polycrystalline thin-film solar cells [19], which showed in a p-type semiconductor with non-shallow acceptor levels, such as p-CdTe with CuCd impurities, the hole density was 5.6 × 10^{14} cm^{-3} under the acceptor concentration of 1.0 × 10^{17} cm^{-3} [19]. The dependence of W on V at various doping densities is also shown in Figure 2.

Table 1. Fermi level E_F, ionized dopants $N_A{}^-$, and V_{bi} in CdTe with different doping densities from 10^{14} to 10^{17} cm^{-3}.

N_A (cm^{-3})	10^{14}	10^{15}	10^{16}	10^{17}
$N_A{}^-$(cm^{-3})	9.07 × 10^{13}	6.05 × 10^{14}	2.61 × 10^{15}	9.16 × 10^{15}
E_F (eV)	0.315	0.267	0.229	0.196
V_{bi} (V)	0.985	1.033	1.071	1.104

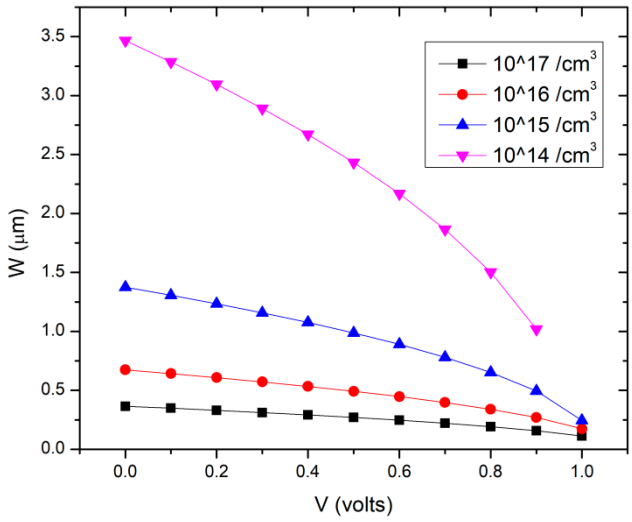

Figure 2. The dependence of W on V at various doping densities.

It can be found that at the solar cell operation voltage of approximately 0.7 V, the depletion width is about 1.8 um in the low doping CdTe film, which can be lowered to 0.1 um in the high doping CdTe film. As the absorption coefficient for CdTe is higher than 10^6 m^{-1} above the absorption edge, and most of the incident light will be absorbed within 1 um depth or less.

2.4. General Solution and Boundary Conditions

The general solution of Equation (3) in the p-type absorber's neutral region is

$$\Delta n(x) = \frac{L_a \tau_n}{{L_n}^2 - {L_a}^2} \phi_0 \exp\left(-\frac{W}{L_a}\right)\left[A\cosh\left(\frac{x}{L_n}\right) + B\sinh\left(\frac{x}{L_n}\right) - \exp\left(-\frac{x}{L_a}\right)\right] \quad (7)$$

where A and B are constants, dependent on the two boundary conditions of the neutral region. We plotted the individual numerical item and the relationship between Δn and x of Equation (7) for a better understanding, as shown in Figures 3 and 4. It can be found that at $x = 0$ (depletion region edge), the dominant parts are $\cosh\left(\frac{x}{L_n}\right)$ and $\exp\left(-\frac{x}{L_a}\right)$ Whereas at $x = H - W$ (back contact), the dominant parts become $\cosh\left(\frac{x}{L_n}\right)$ and $\sin h\left(\frac{x}{L_n}\right)$

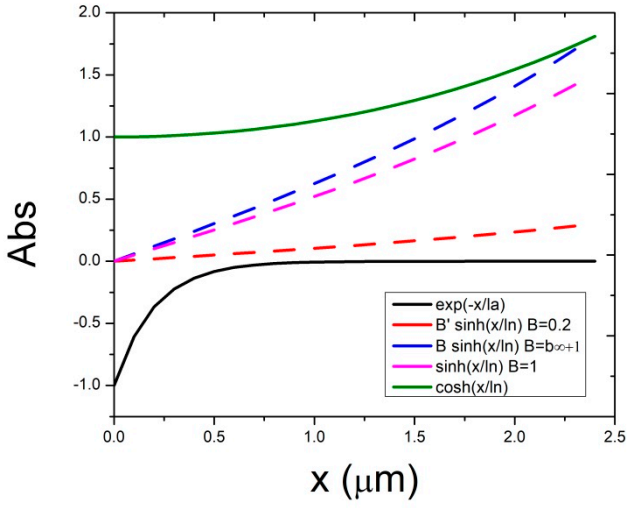

Figure 3. Individual numerical item of the general solution versus x. x is defined as any position in the neutral region.

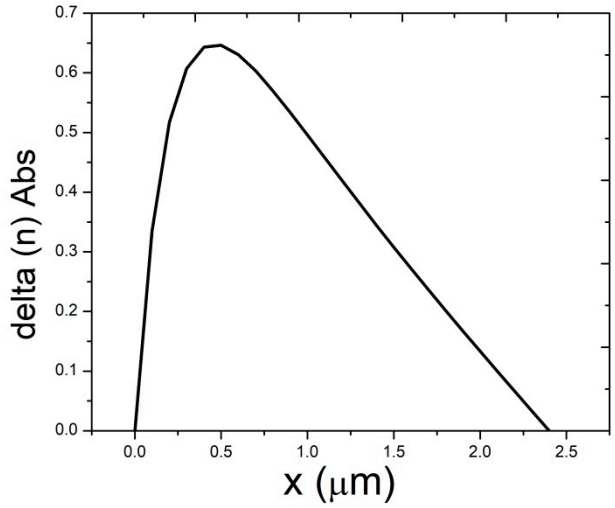

Figure 4. The relationship between Δn and x of the general solution. x is defined as any position in the neutral region. The unit of Δn is cm^{-3}.

(1) At x = 0 (depletion region edge), Δn = 0. The electric field in the depletion region swipes out all the photo-electrons swiftly.
(2) At x = H-W (back contact), Δn = 0. For CdTe cell with p-type ohmic contact, no electron reflector or surface field at the back, we have $S_n = \infty$. As $-D_n \frac{d\Delta n}{dx} = S_n \Delta n$, and $\frac{d\Delta n}{dx} \neq 0$. Therefore, at the back contact, we also have the boundary condition of $\Delta n = 0$.

From the boundary condition at x = 0, we obtain A = 1. To determine the constant B with the boundary condition at the back, we inspect the magnitude of Δn and $\frac{d\Delta n}{dx}$ at x = H − W

$$\Delta n = \frac{L_a \tau_n}{{L_n}^2 - {L_a}^2} \phi_0 \exp\left(-\frac{W}{L_a}\right)\left[\cosh\left(\frac{H-W}{L_n}\right) - (1+b)\sinh\left(\frac{H-W}{L_n}\right) - \exp\left(-\frac{H-W}{L_a}\right)\right] \quad (8)$$

$$\frac{d\Delta n}{dx} = \frac{L_a \tau_n}{{L_n}^2 - {L_a}^2} \phi_0 \exp\left(-\frac{W}{L_a}\right)\left[\frac{1}{L_n}\sinh\left(\frac{H-W}{L_n}\right) - \frac{1+b}{L_n}\cosh\left(\frac{H-W}{L_n}\right) + \frac{1}{L_a}\exp\left(-\frac{H-W}{L_a}\right)\right] \quad (9)$$

Here we replace B with 1 + b and use the expression $L_n = \sqrt{D_n \tau_n}$. Assuming that L_n and H are of the same order, and $H >> L_a$, we can neglect the third term of higher order in the expression of Δn and $\frac{d\Delta n}{dx}$, and have

$$\Delta n = \frac{1}{D_n} \frac{L_a {L_n}^2}{{L_n}^2 - {L_a}^2} \phi_0 \exp\left(-\frac{W}{L_a}\right)\left[\cosh\left(\frac{H-W}{L_n}\right) - (1+b)\sinh\left(\frac{H-W}{L_n}\right)\right] \quad (10)$$

$$\frac{d\Delta n}{dx} = \frac{1}{D_n} \frac{L_a {L_n}^2}{{L_n}^2 - {L_a}^2} \phi_0 \exp\left(-\frac{W}{L_a}\right)\left[\frac{1}{L_n}\sinh\left(\frac{H-W}{L_n}\right) - \frac{1+b}{L_n}\cosh\left(\frac{H-W}{L_n}\right)\right] \quad (11)$$

Therefore, from $\Delta n = 0$, or equivalently $S_n = \infty$ at the back x = $H - W$, we have

$$b = b_\infty = \coth\left(\frac{H-W}{L_n}\right) - 1 \quad (12)$$

The photocurrent density contributed from the neutral p-region J_{NR} is the value of $-qD_n \frac{d\Delta n}{dx}$ at x= 0. Thus,

$$J_{NR} = q\phi_0 \exp\left(-\frac{W}{L_a}\right)\left[\frac{{L_n}^2 L_a}{{L_n}^2 - {L_a}^2}\left(\frac{1}{L_a} - \frac{1+b_\infty}{L_n}\right)\right] \quad (13)$$

Assuming there is no photo-electron loss in the depletion region, the photo-generated carrier collection efficiency in the neutral region is

$$\eta_{NR} = \frac{{L_n}^2 L_a}{{L_n}^2 - {L_a}^2}\left\{\frac{1}{L_a} - \frac{1+\coth\left[\frac{H-W(V)}{L_n}\right]-1}{L_n}\right\} = \frac{L_n^2}{{L_n}^2 - {L_a}^2} - \frac{L_n L_a}{{L_n}^2 - {L_a}^2}\left\{\coth\left[\frac{H-W(V)}{L_n}\right]\right\} \quad (14)$$

The dependence of neutral region photo-carrier collection coefficient on CdTe's diffusion length L_n is shown in Figure 5, assuming H, W, and L_a are 2.5 µm, 0.1 µm, and 0.2 µm, respectively.

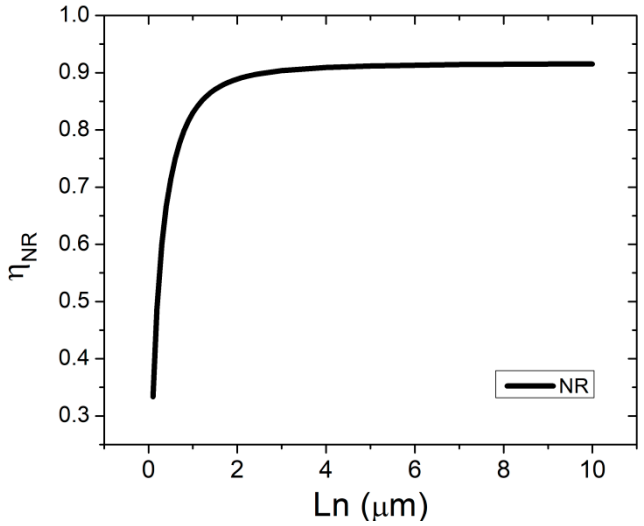

Figure 5. The dependence of neutral region photo-carrier collection coefficient on CdTe's diffusion length L_n.

Thus, the ideal polycrystalline thin-film CdTe solar cell's photo-carrier collection efficiency η_{total} at various doping densities is as shown in Figure 6

$$\eta_{total}(V) = \left[1 - \exp\left(-\frac{W(V)}{L_a}\right)\right] + \exp\left(-\frac{W(V)}{L_a}\right)\left(\frac{L_n^2}{{L_n}^2 - {L_a}^2} - \frac{L_n L_a}{{L_n}^2 - {L_a}^2}\coth\left[\frac{H-W(V)}{L_n}\right]\right) \quad (15)$$

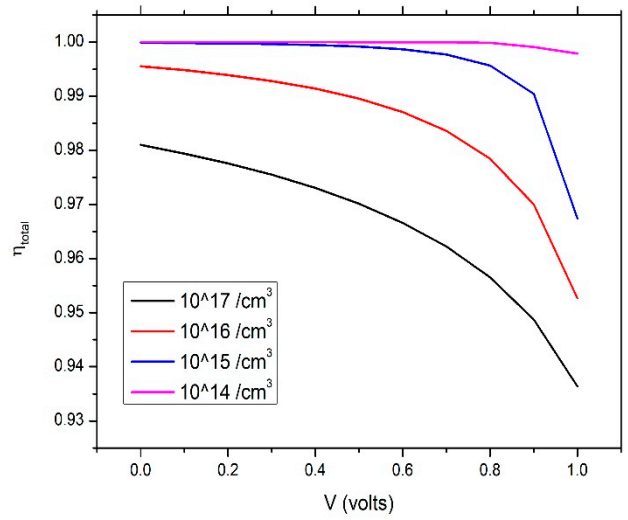

Figure 6. The ideal polycrystalline thin-film CdTe solar cell's photo-carrier collection efficiency at various doping densities.

It is assumed that the collection coefficient of photo-generated current in the depletion region J_W is 100% since there is a strong electric field in the depletion region, which drives

the photo-carriers swiftly without any recombination. The light generated photocurrent density is not constant J_L, or J_{SC}, but bias voltage dependent as described in Equation (16).

$$J_L(V) = q\phi_0\left\{\left[1-\exp\left(-\frac{W(V)}{L_a}\right)\right]+\exp\left(-\frac{W(V)}{L_a}\right)\left(\frac{L_n^2}{{L_n}^2-{L_a}^2}-\frac{L_nL_a}{{L_n}^2-{L_a}^2}\coth\left[\frac{H-W(V)}{L_n}\right]\right)\right\} \quad (16)$$

We also plot the photocurrent at different doping densities of p-type CdTe in Figure 7, and it shows the trend of a much heavier dependence of photocurrent on bias voltage at higher doping density while the photocurrent seems to keep constant at a low doping density of 10^{14} cm^{-3}.

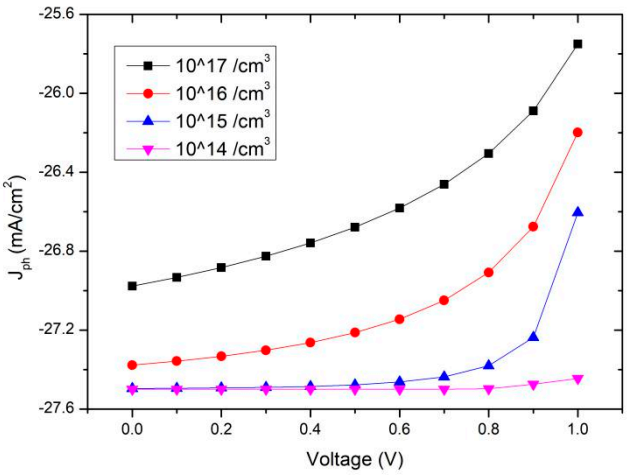

Figure 7. Bias voltage dependence of photocurrent at various doping densities.

3. Comparison of Theory and Experiment

Following Equation (16), we obtain the ideal CdTe solar cell's J-V curve without consideration of any series or shut resistance, which is depicted by

$$J(V) = J_0\left[\exp\left(\frac{qV}{nkT}\right)-1\right]-J_L(V) \quad (17)$$

The model is further validated by using experimental J-V curves from both our lab and James R. Sites [21], as shown in Figures 8 and 9, respectively. It can be found that our model fits very well on James R. Sites' experimental data, but not so good on our data, which may be attributed to the relatively poor device performance compared with James R. Sites (efficiency 13% of our lab vs. 18% of James R. Sites [21]).

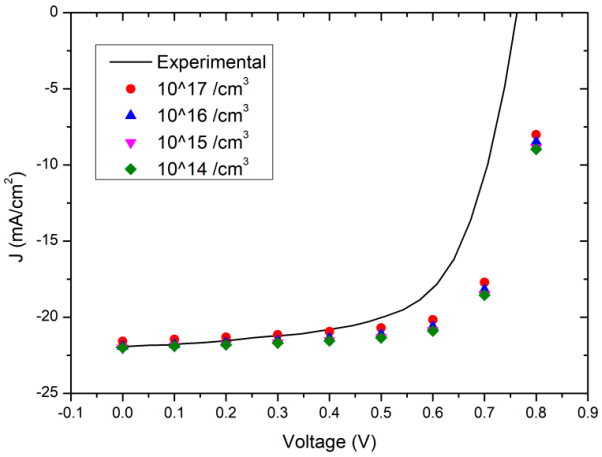

Figure 8. The comparison of our experimental data and theoretical model.

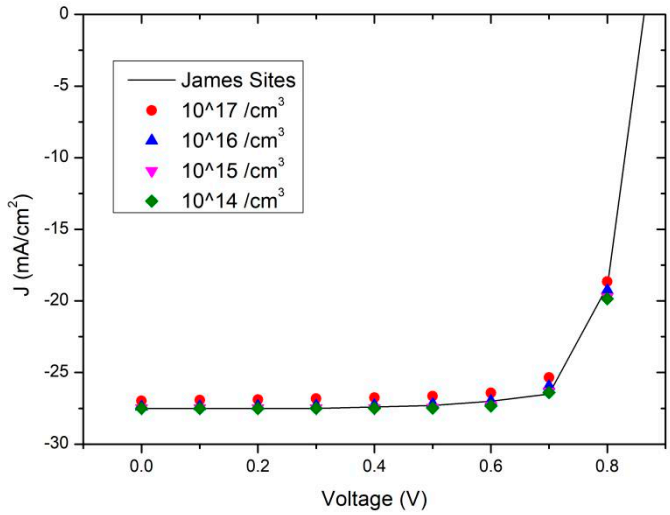

Figure 9. The comparison of experimental data from the other group [21] and our theoretical model.

The model simulations reveal that the photocarrier collection can be improved by increasing the charge carrier diffusion length L_n. For long τ_n and big D_n, a higher η_{total} is obtained, and the collection becomes more effective. Surprisingly, a higher doping density may not be always good for a CdTe solar cell due to the reduced depletion width and decreased photocurrent J_L at normal operation voltage, although the higher doping density can improve the V_{oc} by increasing V_{bi} as indicated in Table 1. When the doping density is extremely big, the depletion width becomes very narrow, leading to a more severe photo-carrier collection loss, since the photo-carriers should be generated primarily within, or very near to the depletion region when the solar cell is biased at high bias voltage.

The more recent experiments from First Solar involved various combinations of p-type back contact materials, buffer layers, and front window layers, in order to create an energy barrier or other obstacle to the movement of electrons, and therefore reduce the electron diffusion to the back contact. Our model is one of the most classic device configurations of CdTe thin-film solar cells, and in the future, it can be extended by adding energy barriers in the front and back sides. Furthermore, the surface recombination velocity S_n at the metal back contact is assumed to be infinite in our model, which can be changed to a non-infinite value in the existence of a back surface field, that is, by the deposition of ZnTeCu.

4. Conclusions

A theoretical model for CdTe solar cells is developed to describe the voltage-dependent charge carrier collection phenomenon. We solved the diffusion equations with boundary conditions in the neutral region and obtained the analytical expression of the bias-dependent photocurrent collection in terms of depletion width, diffusion length, and absorption length. Moreover, we validated our model by employing both simulation and experimental data in forward bias. It was found that a longer charge carrier diffusion length can improve the carrier collection efficiency, and a higher doping density may not be good for CdTe solar cells due to the reduced depletion width and decreased photocurrent. This model can be used further to understand the device physics, predict the device performance and calculate the device parameters including the surface recombination speed in the back contact.

Author Contributions: Both authors contribute equally to the manuscript. Writing—original draft preparation, C.X.Z.; Writing—review and editing, K.K.C. Both authors have read and agreed to the published version of the manuscript.

Funding: This research received no external funding.

Institutional Review Board Statement: Not applicable.

Informed Consent Statement: Not applicable.

Acknowledgments: This work was supported by the China Triumph International Engineering Company.

Conflicts of Interest: The authors declare no conflict of interest.

References

1. Hegedus, S.; Desai, D.; Thompson, C. Voltage dependent photocurrent collection in CdTe/CdS solar cells. *Prog. Photovolt. Res. Appl.* **2007**, *15*, 587–602. [CrossRef]
2. Mitchell, K.W.; Fahrenbruch, A.L.; Bube, R.H. Evaluation of the CdS/CdTe heterojunction solar cell. *J. Appl. Phys.* **1977**, *48*, 4365–4371. [CrossRef]
3. Eron, M.; Rothwarf, A. Effects of a voltage-dependent light-generated current on solar cell measurements: CuInSe2/Cd(Zn)S. *Appl. Phys. Lett.* **1984**, *44*, 131–133. [CrossRef]
4. Liu, X.X.; Sites, J.R. Solar-cell collection efficiency and its variation with voltage. *J. Appl. Phys.* **1994**, *75*, 577–581. [CrossRef]
5. Ali, B.; Murray, R.; Hegedus, S.S.; Shah. S.I. Analysis of voltage and temperature dependent photocurrent collection in p3ht/pcbm solar cells. *J. Appl. Phys.* **2012**, *112*, 114514. [CrossRef]
6. Dawidowski, W.; Ściana, B.; Zborowska-Lindert, I.; Mikolášek, M.; Kováč, J.; Tłaczała, M. Tunnel junction limited performance of InGaAsN/GaAs tandem solar cell. *Sol. Energy* **2021**, *214*, 632–641. [CrossRef]
7. Gloeckler, M.; Jenkins, C.R.; Sites, J.R. Explanation of Light/Dark Superposition Failure in CIGS Solar Cells. *MRS Proc.* **2003**, *763*, B5.20. [CrossRef]
8. Moore, J.E.; Dongaonkar, S.; Chavali, R.V.K.; Alam, M.A.; Lundstrom, M.S. Correlation of Built-In Potential and I–V Crossover in Thin-Film Solar Cells. *IEEE J. Photovolt.* **2014**, *4*, 1138–1148. [CrossRef]
9. Sun, X.; Asadpour, R.; Nie, W.; Mohite, A.D.; Alam, M.A. A Physics-Based Analytical Model for Perovskite Solar Cells [Sep 15 1389-1394]. *IEEE J. Photovolt.* **2016**, *6*, 1390. [CrossRef]
10. Hejri, M.; Mokhtari, H.; Azizian, M.R.; Ghandhari, M.; Söder, L. On the Parameter Extraction of a Five-Parameter Double-Diode Model of Photovoltaic Cells and Modules. *IEEE J. Photovolt.* **2014**, *4*, 915–923. [CrossRef]
11. Paul, S.; Sohal, S.; Swartz, C.; Li, D.B.; Bista, S.S.; Grice, C.R.; Li, J.V. Effects of post-deposition CdCl2 annealing on electronic properties of CdTe solar cells. *Sol. Energy* **2020**, *211*, 938–948. [CrossRef]
12. Li, D.; Song, Z.; Awni, R.A.; Bista, S.S.; Shrestha, N.; Grice, C.R.; Yan, Y. Eliminating S-Kink To Maximize the Performance of MgZnO/CdTe Solar Cells. *ACS Appl. Energy Mater.* **2019**, *2*, 2896–2903. [CrossRef]
13. Song, T.; Kanevce, A.; Sites, J.R. Emitter/absorber interface of CdTe solar cells. *J. Appl. Phys.* **2016**, *119*, 233104. [CrossRef]
14. Paul, S.; Swartz, C.; Sohal, S.; Grice, C.; Bista, S.S.; Li, D.B.; Li, J.V. Buffer/absorber interface recombination reduction and improvement of back-contact barrier height in CdTe solar cells. *Thin Solid Film.* **2019**, *685*, 385–392. [CrossRef]
15. Swartz, C.H.; Rab, S.R.; Paul, S.; van Hest, M.F.; Dou, B.; Luther, J.M.; Li, J.V. Measurement of band offsets and shunt resistance in CdTe solar cells through temperature and intensity dependence of open circuit voltage and photoluminescence. *Sol. Energy* **2019**, *189*, 389–397. [CrossRef]
16. Kalogirou, S.A. (Ed.) Dedication. In *McEvoy's Handbook of Photovoltaics*, 3rd ed.; Academic Press: Cambridge, MA, USA, 2018; p. v.
17. Chin, K.K. Dual roles of doping and trapping of semiconductor defect levels and their ramification to thin film photovoltaics. *J. Appl. Phys.* **2012**, *111*, 104509. [CrossRef]
18. Perrenoud, J.; Kranz, L.; Gretener, C.; Pianezzi, F.; Nishiwaki, S.; Buecheler, S.; Tiwari, A.N. A comprehensive picture of Cu doping in CdTe solar cells. *J. Appl. Phys.* **2013**, *114*, 174505. [CrossRef]
19. Chin, K.K. p-Doping limit and donor compensation in CdTe polycrystalline thin film solar cells. *Sol. Energy Mater. Sol. Cells* **2010**, *94*, 1627–1629. [CrossRef]
20. Hädrich, M.; Metzner, H.; Reislöhner, U.; Kraft, C. Modelling the quantum efficiency of cadmium telluride solar cells. *Sol. Energy Mater. Sol. Cells* **2011**, *95*, 887–893. [CrossRef]
21. Sites, J.; Munshi, A.; Kephart, J.; Swanson, D.; Sampath, W.S. Progress and challenges with CdTe cell efficiency. In Proceedings of the 2016 IEEE 43rd Photovoltaic Specialists Conference (PVSC), Portland, OR, USA, 5–10 June 2016; IEEE: New York, NY, USA, 2016.